JOURNAL OF OPTOELECTRONICS AND ADVANCED MATERIALS Vol. 10, No. 8, August 2008, p. 1927 - 1932

Formation of plasma from pure and polymer-doped water ice during intense laser irradiation

A. MATEI[a,b], J. SCHOU[a,*], K. RODRIGO[c], M. DINESCU[b], R. PEDRYS[d]
[a]*Department of Photonics Engineering, Risø Campus, Technical University of Denmark, DK-4000 Roskilde, Denmark.*
[b]*National Institute for Laser, Plasma and Radiation Physics, PO Box MG–16 Magurele, RO-077125 Bucharest, Romania*
[c]*Fuel Cells and Solid State Chemistry Department, Risø National Laboratory, Technical University of Denmark, DK-4000 Roskilde, Denmark*
[d]*Institute of Physics, Jagiellonian University, PL-30 019 Krakow, Poland*

Ice produced from ultrapure water or with 1 % polyethylene glycol (PEG) was irradiated by laser light with fluences between 2 and 80 J/cm^2 in the ultraviolet (UV) regime at 355 nm and in the infrared (IR) regime at 1064 nm. The laser light induces a visible plasma above a fluence of 3.5 J/cm^2 in the UV regime and above 8.5 J/cm^2 in the IR regime. The ions from the plasma plume were studied by a Langmuir probe. The behavior of the plasma current can be understood in terms of ionization breakdown at the ice surface.

(Received March 1, 2008; accepted June 30, 2008)

Keywords: Plasma, ablation plume, Water ice, PEG, MAPLE

1. Introduction

Plasma formation during intense laser irradiation of solids is a complex phenomenon, which occurs during processing of materials [1], chemical analysis by laser ablation [2], film production by pulsed laser deposition (PLD) [3,4] and laser tissue-interactions [5]. Laser-induced plasmas can be formed not only from surfaces, but also in a closed volume exposed to a focused laser beam, for example in microsurgery [5,6].

Water ice is a solid which apart from the density (pure ice ~ 0.93 g/cm^3 depending on structure and preparation [7]) resembles liquid water which is the main constituent of tissue. It has been used as host for salts in desorption studies [8,9] as well as a potential matrix for biomolecules in MALDI (Matrix assisted laser desorption ionization) [10]. A current interest is to use water ice as a matrix for the MAPLE (Matrix assisted pulsed laser evaporation) technique for the production of thin films of organic materials [11,12]. In MAPLE a frozen solvent with a few per cent of a material to be deposited is irradiated by a laser in a vacuum chamber, such that the frozen matrix undergoes an "explosive" evaporation. The volatile solvent is pumped away, while the solute, i.e. the film material, is deposited on a suitable substrate. The idea in MAPLE is that the matrix absorbs the laser energy such that any damage on the solute is reduced or avoided, and subsequently converted to translational energy for the ejection of molecules from the solute and the matrix. A second important point is that the matrix molecules do not interact photochemically with the "film" molecules.

Water ice has been used successfully as a matrix for bioorganic molecules in several cases [13-15]. However, most of the systematic studies have been performed for the polymer, PEG (polyethylene glycol), which has been a model system for MAPLE [16-20]. In particular, Bubb et al. [16] showed that the PEG molecules from water ice were exposed to fewer photochemical modifications than PEG in $CHCl_3$ during film deposition by MAPLE, and water ice thus is an attractive matrix. The deposition of PEG was accompanied by a plasma for fluences above 3.5 J/cm^2 [18], but nevertheless it turned out that a film of partly intact molecules was formed on a substrate even for a relatively high fluence of 5 J/cm^2 with MAPLE deposition [20].

We have investigated the plasma from water ice surfaces in order to identify the mechanism of plasma formation. Since the results at the laser wavelength in the UV regime at 355 nm were not sufficiently conclusive [18], we have recently extended the measurements to the IR regime at 1064 nm [19]. The present work shows that the behavior of the laser-induced plasma from water ice is similar to that reported in ionization breakdown for laser-tissue interactions [5].

2. Experimental.

The experiments have been carried out at the MAPLE setup at Risø National Laboratory [18-20]. The duration of the laser pulse was 6-7 ns and the fluence was varied between 3 and 80 J/cm^2 (corresponding to an intensity I from 4×10^8 W/cm^2 to 1×10^{10} W/cm^2). The area of the elliptical laser beam spot ranged from 0.006 cm^2 to 0.025 cm^2. The laser beam was directed at an angle of 45^o with respect to the normal onto a rotating ice target in a chamber with a base pressure of 10^{-6} mbar (Fig.1). The

setup has been modified such that the same ice target could be irradiated by two beams at 355 nm and 1064 nm from the same Nd:YAG laser in a sequence just by exchanging the coated vacuum window in a small load lock system [19]. However, usually the measurements at the UV and IR wavelength were carried out in separate runs.

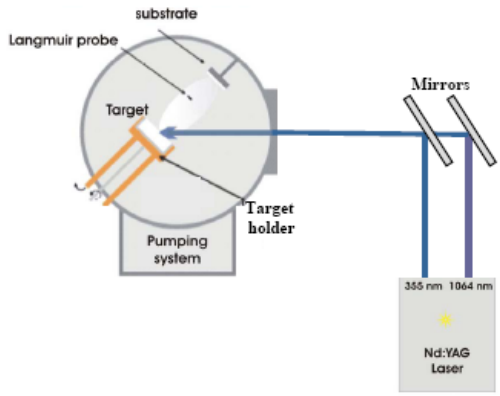

Fig. 1 . The experimental setup at Risø National Laboratory

The target was a flash-frozen ice matrix made from a solution which was poured into a copper cup cooled to liquid nitrogen temperature and then kept in liquid nitrogen for 10 minutes. The solution consisted of 1% weight PEG (Aldrich, average molecular weight: 1500 g/mole), which was dissolved in ultrapure water (spec. resistivity > 18 MΩcm) at room temperature and homogenized by an ultrasound bath for 5 minutes prior to the freezing procedure. Finally, the target cup of 20-mm-diameter and a depth of 6 mm with the ice matrix was inserted into the cryogenic target holder system in the vacuum chamber and kept at – 50 ^{o}C.

The ion current from the ablation plume was measured with a planar Langmuir probe similar to those in Ref. [21]. The probe was a 2.1×2.3 mm^2-rectangular copper plate insulated on the rear, oriented to face the target spot and placed 35 mm from the target with an angle of 8^{o} with respect to the normal. Usually, the ion time-of-flight (TOF) spectra as well as the measurements of the integrated current density on the probe were taken with a bias of -30 V. In contrast to the ion current results from Ref. [18] which were obtained as an average over 5 pulses (after a cleaning sequence with 5 pulses), it was only possible to record a single TOF spectrum at 1064 nm on each spot. The high heat load at 1064 nm made the ice surface transparent, and the subsequent signals were hardly measurable. Since also the signals at 355 nm were decreasing with shot number down to about 60 % of the first signal after the first 5 shots, the absolute difference between the signals at 355 nm and 1064 nm is somewhat larger than indicated in the figures, but this does not influence the general trend.

Characteristic TOF-spectra from pure water ice for a fluence range of 8.5-73.5 J/cm^2 at 1064 nm are shown in Fig. 2. There is no signal for the 8.5 J/cm^2 which actually is the threshold for ion emission. Each signal can be integrated to yield the charge per shot collected over the area of the probe, i. e. charge density.

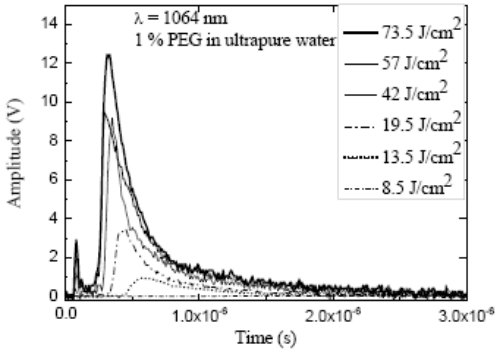

Fig. 2. Time-of-flight (TOF) spectra 1 wt% PEG in water ice produced on a beam spot area of 0.006 cm^2 at the wavelength 1064 nm. Target-probe distance: 35 mm, probe bias: - 30 V. breakdown happens.

The charge density as a function of bias at a fluence of 49.5 J/cm^2 at 1064 nm is shown in Fig. 3. It appears there is no further enhancement of the current density for bias values less than - 30 V. The same trend has been observed for laser irradiation at 355 nm. Therefore, this value of the bias has been used for all measurements on pure and polymer-doped ice, even though the trend is similar for the measurements with – 10 V. This value is slightly larger than that used for laser ablation plumes from metals with cylindrical probes (- 40 V) [22], but less than that used for the measurements of TOF spectra from silver in background gases with a planar probes (-10 V) [23].

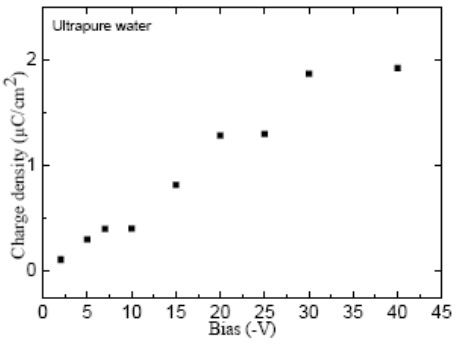

Fig. 3. Charge density per shot as a function of bias for ultrapure ice at a fluence of 49 J/cm^2. Laser wavelength: 1064 nm, target-probe distance 35 mm, beam spot area: 0.006 cm^2.

3. Results and discussion: ion current measurements

The TOF-spectra in Fig. 2 show a distinct ion signal with a peak in the time range from 300 ns to 600 ns. The small peak around 100 ns consists of photo-electrons that are emitted from the probe because of the strong emission of UV light from the plume during the initial expansion.

The height of the peak as well as the total current obtained as an integral over the spectra in Fig. 2 increase with fluence. This trend is similar to that reported for the laser-induced plasma in the UV regime reported in refs. [18,24]. At the threshold for ion emission at 8.5 J/cm^2 there is no discernable signal. The velocity of the ions in the peak increases with fluence from 60 km/s up to 110 km/s. At 110 km/s the oxygen ions have a kinetic energy of ~ 1000 eV and the hydrogen ions an energy of ~ 60 eV. Similar, but slightly smaller velocities were found for laser irradiation at 355 m as well [18].

An important point is whether or not the signal from water ice is changed as a result of the polymer doping. In Fig. 4 the collected charge density from polymer-doped and pure ice is shown as a function of fluence for laser irradiation at 355 nm. One notes that there is a threshold for ion emission at 3.5 J/cm^2 at this wavelength, and a strong enhancement of the ion signal above the threshold as also reported in ref. [18]. From Fig. 4 it can be seen that there might be a slight increase of the current density for the data points obtained from water ice with PEG compared with a pure ice matrix. This tendency is also observed in the IR regime at 1064 nm. As discussed later, this can be explained by a higher density of seed electrons in additional defects and at fragments of the polymer in the ice.

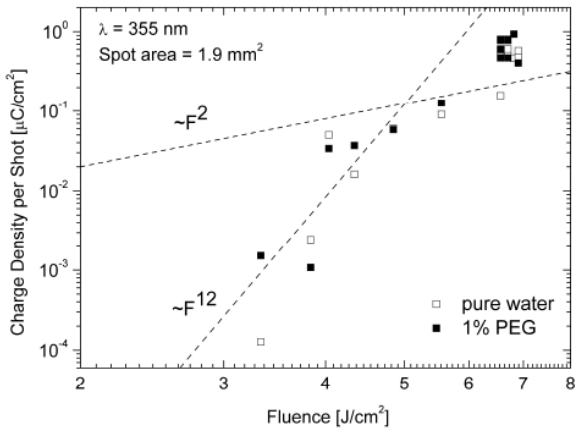

Fig. 4. Charge density per shot for 1 wt % PEG in water ice and pure water ice as a function of fluence F at the wavelength 355 nm. target-probe distance 35 mm, beam spot area: 0.019 cm^2, bias. - 30 V. The dashed lines indicate a behavior proportional to F^2 and F^{12},

The velocity of the ions from the smallest beam spot in Fig. 5 is significantly higher. This tendency has also been observed for laser irradiation at 355 nm. We are currently working on models which can explain this tendency.

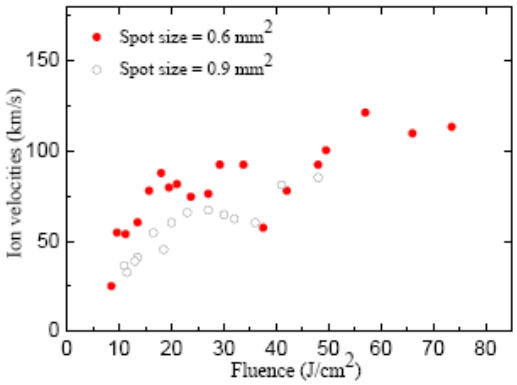

Fig. 5. The velocity of the ions in the peak of the TOF-spectra from 1 wt % PEG in water ice as a function of fluence for two laser beam spot sizes at 1064 nm. Target-probe distance 35 mm, bias: - 30 V.

A critical point for the study of the fluence dependence recorded in a relative small solid angle (5.3 10^{-4} sr) in forward direction around the normal of the target is whether or not the angular distribution changes significantly in the fluence range considered. In the low end of the range from 1.6 to 6.6 J/cm^2 Weaver and Lewis [25] found very small variations at the wavelength 532 nm, and in the upper part of the range Thum-Jäger and Rohr [26] found only little variation in the angular behavior from 20 to 180 J/cm^2 in the IR regime at 1064 nm. Also Gorbunov and Konov [27] found only a weak dependence on the angular distribution in the UV regime at 308 nm for a fluence between 60 and 140 J/cm^2. Since the data from the current measurements increase by more than two orders of magnitude in the fluence range considered, the error introduced by any variation of the angular distribution is insignificant compared with the experimental uncertaincy.

From another point of view, one may consider that the angular distribution is determined by the initial plume distribution according to the hydrodynamic model of Anisimov et al. [4, 28, 29]. Strictly speaking, this model does not account for plasma formation, but it was shown that the angular distribution of a plasma plume from silver can be well described by Anisimov's model with a value of the adiabatic constant $\gamma = 1.25$ [4, 29, 30]. When the laser pulse is terminated, the position of the front is determined roughly by the velocity of the ions in the front. Using the data from Fig. 5 for the front velocity we can estimate that the plume front has propagated between 40 and 70 μm from the surface after a pulse duration of 6-7 ns. Since the area of the beam spot can be approximated by a circle of radius 0.45-0.55 mm, the ratio between the front distance of the initial plume and the radius varies at

most a factor of 2 (see arguments in Ref. [28]). Also this estimate leads to the conclusion that the variation of the angular distribution is insignificant compared with the experimental uncertainty.

4. Origin of plasma production

As discussed elsewhere, the absorption depth $1/\alpha \approx 0.15$ cm for 355 nm [18,31]. Unfortunately, it was not possible to determine the corresponding value for 1064 nm, but since the attenuation is primarily controlled by nonlinear absorption processes as mentioned in [32], we assume that the absorption depth is of the same order of magnitude as the one for 355 nm. This depth is much larger than the evaporation depth d for a typical beam spot of 0.015 cm^2. With the value of the cohesive energy 0.45 eV/molec. from Sack and Baragiola [33] one obtains a value for d of about 7 μm for a fluence of 2 J/cm^2. With increasing fluence this value increases to 300 μm at 80 J/cm^2. Since the assumption of this estimate is that the laser energy is spent solely on an evaporation process, and the ionization of a water molecule requires 12.6 eV, the actual depth of an ablation crater can be one order of magnitude smaller.

The laser light at 355 nm and 1064 can only be absorbed in flash-frozen ice with a lot of cracks, bubbles and other defect sites. Since these defects act as traps for seed electrons, the picture is that these electrons are accelerated by inverse bremssstrahlung from the strong laser field and generate new electrons in an avalanche process (Fig. 6). At 355 nm a three-photon process leads to excitation of an electron to the conduction band and direct photoemission as well, since the threshold for this process is about 10 eV (see references: in [18]). These three-photon processes accelerate the avalanche so that a high a value of the "free" electron density is reached faster at 355 nm than at 1064 nm.

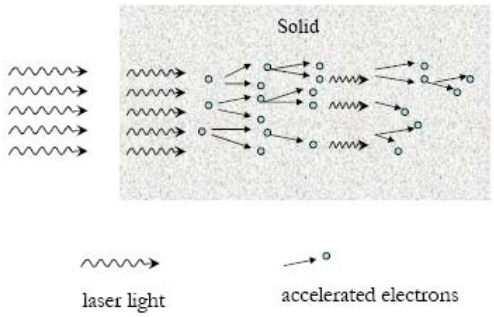

Fig. 6. Schematic view of avalanche ionization. The laser light hits the solid at the left-hand side.

In contrast to the fast energy transfer from electrons to the lattice which takes place in metals on ps scale [34,35], much of the energy in an insulator as water ice is initially stored as (localized) ionizations and excitations of water molecules. This energy is then converted to atomic motion and lattice heat via dissociative recombinations and repulsive transitions similar to processes that take place at electronic sputtering with ions or electrons [36,37]. These transitions happen during a ns-scale, while the electron-atoms collisions take place immediately. Since these processes are of statistical nature, a picture of the irradiated ice emerges: small microvolumes of plasma are generated directly at defects, where the highest density of seed electrons originally was, e.g. along the cracks and around the bubbles. The (micro) plasmas are formed directly in the solid ice and expand initially in all directions. In the other part of the irradiated ice, where the initial seed electron density is low, the heating proceeds via the molecular transitions. In these volumes the water (ice) will gradually reach a supercritical state or proceed via phase explosion as a neutral flow [38, 39, 40], until it is mixed into plasma branches of the ablation plume. The slowest part of the plume will consists of predominantly neutral water molecules evaporated from cold pockets, but these particles are not recorded by the Langmuir probe. At the lowest fluences discussed here also aggregates of polymers embedded in neutral water molecules are transferred out of the plume to a substrate [20,32,39]. However, at higher fluence an increasing fraction of the plume particles become decomposed and ionized.

This picture has a clear analogy with the ionization breakdown that occurs in water at a high laser intensity [5,6]. With increasing intensity the plasma formation starts as a luminous plasma in a cavitation bubble exactly at the waist of a focused laser beam, i.e. at the point, where the laser intensity reaches it maximum [5]. In a comprehensive series of papers, Vogel and collaborators [5, 41, 42] have modeled the generation of free electrons in water on the basis of a rate equation which accounts for multiphoton production of free electrons, cascade production of electrons, loss of electrons by diffusion out of the focal volume and recombination. The authors have calculated the threshold for ionization breakdown for different pulse lengths from 100 fs to 6 ns and for different wavelengths from 1064 nm to 355 nm. They assumed that ionization breakdown starts at the critical “free” electron density $\rho = 1\times 10^{20}$ electrons/cm^3, an ionization value for water from an amorphous semiconductor (I_{pot} = 6.5 eV) suggested by Sacchi [42] and obtained good agreement with their experiments [5,41]. The result of their calculation is shown in the lower panel of Fig. 7. The important trend is that for laser light at 355 nm multiphoton processes produce an additional number of seed electrons which again are accelerated by inverse bremsstrahlung. Therefore, the production of free electrons increases gradually with intensity I. Also the threshold for ionization breakdown is reached at a lower intensity, since more seed electrons are available. In contrast, the breakdown at 1064 nm is only reached via avalanche ionization, and the sharp threshold occurs at a higher intensity than that for 355 nm. As expected from ref. [5], the electron density is a linear function of I at high intensities for both wavelengths. A convincing argument

for avalanche ionization in both cases is the similar TOF-spectrum taken from the same ice target at 8.2 J/cm^2 at 355 nm and 14 J/cm^2 at 1064 nm [19].

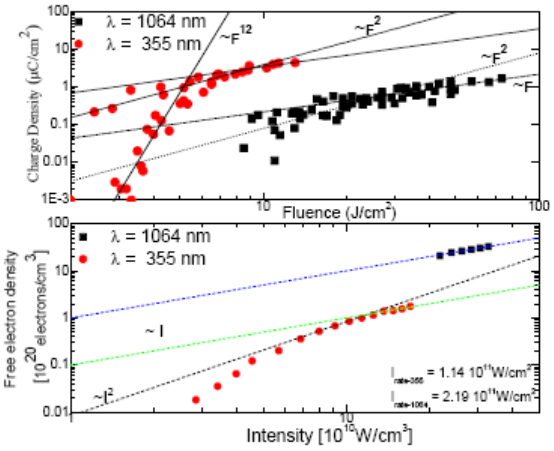

Fig. 7. Upper panel) Data for the charge density at 355 nm and 1064 as a function of fluence. All data taken for a target-probe distance of 35 mm and a bias of -30 V. The fluence dependence is indicated with thin lines. Lower panel) Modeling results of the free electron density in water as a function of laser intensity I [41] for IR and UV irradiation. Ionization breakdown is assumed to occur at 10^{20} electrons/cm^3. I-rate indicates for which intensity the ionization

The collected charge density is depicted as a function of fluence *F* (equivalent to intensity since the pulse length is similar for both wavelengths) in the upper panel. The behavior is similar to that shown in the lower panel, since the threshold for plasma formation is much lower at 355 nm than at 1064 nm, the threshold is sharper for 1064 nm and the density for both wavelengths approaches a linear dependence on fluence. The fact that the current density is higher for 355 nm than that for 1064 nm can be ascribed to the low value of the ionization potential (6.5 eV) in the calculations for water ice. Finally, this picture is supported by the data in Fig. 4, where the charge density is slightly higher for water ice matrices with PEG than those without PEG. The PEG molecules are in this respect an "impurity" which provides additional seed electrons for the ionization breakdown.

5. Conclusion

The plasma from laser-irradiated ice has been investigated in the UV and IR regime within a fluence range of 2 – 80 J/cm^2. The current density measured for both 355 nm and 1064 follows the same trend as the intensity dependence for ionization breakdown in water known from laser-tissue interactions. While the breakdown in IR exclusively is caused by avalanche ionization assisted by seed electrons in crack and bubbles, additional seed electrons are produced by multi-photon processes at 355 nm. In general, the measured the current density is much smaller for IR irradiation than for UV irradiation. The plasma current from PEG-doped ice seems to be slightly larger than that from pure ice. The velocity of the ions in the peak of the TOF-spectra increases from 35 to 110 km/s with fluence.

Acknowledgement

This research has been supported by a Marie Curie Fellowship of the European Community programme Marie Curie Host Fellowship under contract number HPMT-CT-2001-00402-04 and HPMT-CT-2001-00402-10. The authors appreciate discussions with A. Vogel. The authors acknowledge the competent technical assistance from Arne Nordskov.

References

[1] D. Bäuerle, Laser processing and chemistry, Springer-Berlin (2000).
[2] R. E. Russo, X. Mao, in Laser Ablation and Desorption, edited by J. C. Miller and R. F. Haglund, Experimental Methods in the Physical Sciences vol. 30. (Academic Press, New York, 1998) p. 375.
[3] D. H. Lowndes, in Laser Ablation and Desorption, edited by J. C. Miller and R. F. Haglund, Experimental Methods in the Physical Sciences vol. 30. (Academic Press, New York, 1998) p. 475.
[4] J. Schou, S. Amoruso, J. G. Lunney, in: Laser ablation and its applications, Ed. C. Phipps, Springer, New York (2007), p. 67.
[5] A. Vogel, V. Venugopalan, Chem. Rev. **103,** 577 (2003).
[6] A. Vogel, J. Noack, G. Hüttman, G. Paltauf, Appl. Phys. B **81,** 1015 (2005).
[7] P. Jenniskens, D. F. Blake and A. Kouchi, in: Solar System Ices, edited by B. Schmitt, C. de Bergh and M. Feston (Kluwer Academics, Dordrecht, 1998) p. 139.
[8] C. Focsa, J. L. Destombes, Chem. Phys. Lett. **347,** 390 (2001).
[9] C. Mihesan, M .Ziskind, B. Chazallon, E. Therssen, P. Degroux, C. Focsa, Surf. Sci. **593**, 221 (2005).
[10] M. L. Baltz-Knorr, K. E. Skriver and R. F. Haglund, Jr., Appl. Surf. Sci. **197-198**, 11 (2002).
[11] D. B. Chrisey, A. Piqué, R. A. McGill, J. S. Horwitz, B. R. Ringeisen, D. M. Bubb, P. K. Wu, Chem. Rev. **103,** 553 (2003).
[12] A. Piqué, 2007. in: Pulsed Laser Deposition of Thin Films, ed. R. Eason Wiley, Hoboken, (2007), p. 63.
[13] B. R. Ringeisen, J. Callahan, P. K. Wu, A. Piqué, B. Spargo, R. A. McGill, M. Bucaro, H. Kim, D. M. Bubb, D. B. Chrisey, Langmuir **17**, 3472 (2001).
[14] J. I. Berry, S. Sun, Y. Dou, A. Wucher, N. Winograd, Anal. Chem. **75**, 5146 (2003).
[15] A. Purice, J. Schou, P. Kingshott and M. Dinescu.

Chem. Phys. Lett. **435**, 350 (2007).
[16] D. M. Bubb, P. K. Wu, J. S. Horwitz, J. H. Callahan, M. Galicia, A. Vertes, R. A. McGill, E. J. Houser, B. R. Ringeisen, D. B. Chrisey, J. Appl. Phys. **91**, 2055 (2002).
[17] D. Bubb, B. R. Ringeisen, J. H. Callahan, M. Galicia, A. Vertes, J. S. Horwitz, R. A. McGill, E. J. Houser, P. K. Wu, A. Piqué, D. B. Chrisey, Appl. Phys. A **73**,121 (2001).
[18] K. Rodrigo, B. Toftmann, J. Schou, R. Pedrys, Chem. Phys. Lett. **399**, 368 (2004).
[19] A. Purice, J. Schou and M. Dinescu, Chem. Phys. Lett. **427**, 251 (2006).
[20] B. Toftmann, K. Rodrigo, J. Schou and R. Pedrys, Appl. Surf. Sci. **247**, 211 (2005).
[21] B. Toftmann, J. Schou, T. N. Hansen and J.G. Lunney, Phys. Rev. Lett. **84**, 3998 (2000).
[22] B. Thestrup, B. Toftmann, J. Schou, B. Doggett and J. G. Lunney, Appl. Surf. Sci. **197-199**, 175 (2002).
[23] S. Amoruso, B. Toftmann and J. Schou, Phys. Rev. E **69**, 056403 (2004).
[24] P. E. Dyer, Appl. Phys. Lett. **33**, 1630 (1989).
[25] I. Weaver and C. L. S. Lewis, J. Appl. Phys. **79**, 7216 (1996).
[26] A. Thum-Jäger, K. Rohr, J. Phys. D: Appl. Phys. **32**, 2831 (1999).
[27] A. A. Gorbunov, V. I. Konov, Sov. Phys. Tech. Phys. **59**,1271 (1989).
[28] S. I. Anisimov, D. Bäuerle and B. Luk'yanchuk, Phys. Rev. B **48,** 12 076 (1993).
[29] B. Toftmann, J. Schou and J.G. Lunney, Phys. Rev. B **67**, 104101 (2003).
[30] T. N. Hansen, J. Schou and J.G. Lunney, Appl. Phys. A **69**, S601 (1999).
[31] J. Schou, in: Proceedings of the Nato Advanced Institute in Sinaia, 2007, ed. Ashok K. Vaseashta (to be published).
[32] A. L. Mercado, C. E. Allmond, J. G. Hoekstra and J. M. Fitz-Gerald, Appl. Phys. A **81**, 591 (2005).
[33] N. J. Sack and R. A. Baragiola, Phys. Rev. B **48**, 9977 (1993).
[34] K. Vespentoft and P. Balling, Appl. Phys. A **84**, 207 (2006).
[35] D. S. Ivanov and L. V. Zhigilei, Phys. Rev. B **71**, 165417 (2005).
[36] R. A. Baragiola, R. A . Vidal, W. Svendsen, J. Schou, M. Shi, D. A. Bahr, C. L. Atteberry, Nucl. Instr. Meth. B **209**, 294 (2003).
[37] J. Schou, Nucl. Instr. Meth. B **27**, 188 (1987).
[38] D. Perez, L. J. Lewis, P. Lorazo, M. Meunier, Appl. Phys. Lett. **89**, 141907 (2006)
[39] E. Leveugle, L. V. Zhigilei, J. Appl. Phys. **102**, 074914 (2007).
[40] Q. Lu, Phys. Rev. E **76**, 016410 (2003).
[41] A. Vogel and J. Noack, SPIE-Proc. 4260, " Functional Imaging and Optical Manipulation of Living Cells and Tissue" (2001) p. 83.
[42] J. Noack, A. Vogel, IEEE J. Quant. Electr. **34**, 1156 (1999).
[43] C. A. Sacchi, J. Opt. Soc. Am. B **8**, 337 (1991).

*Corresponding author. j.schou@risoe.dk